AIAA-95-0832

The Effects of Vortex Modeling on Blade-Vortex Interaction Noise Prediction

J.M. Gallman, and C. Tung
U.S. Army Aeroflightdynamics Directorate
NASA Ames Research Center
Moffett Field, CA
S.L. Low
Sterling Federal Systems
NASA Ames Research Center
Moffett Field, CA

33rd Aerospace Sciences Meeting and Exhibit
January 9-12, 1995 / Reno, NV

The Effects of Vortex Modeling on Blade-Vortex Interaction Noise Prediction

Judith M. Gallman, * Chee Tung*
US Army Aeroflightdynamics Directorate, ATCOM
NASA Ames Research Center, Moffett Field, California

Scott L. Low*
Sterling Federal Systems
NASA Ames Research Center, Moffett Field, California

Abstract

The use of a blade vortex interaction noise prediction scheme, based on CAMRAD/JA, FPR and RAPP, quantifies the effects of errors and assumptions in the modeling of the helicopter's shed vortex on the acoustic predictions. CAMRAD/JA computes the wake geometry and inflow angles that are used in FPR to solve for the aerodynamic surface pressures. RAPP uses these surface pressures to predict the acoustic pressure. Both CAMRAD/JA and FPR utilize the Biot-Savart Law to determine the influence of the vortical velocities on the blade loading and both codes use an algebraic vortex model for the solid body rotation of the vortex core. Large changes in the specification of the vortex core size do not change the inplane wake geometry calculated by CAMRAD/JA and only slighty affect the out-of-plane wake geometry. However, the aerodynamic surface pressure calculated by FPR changes in both magnitude and character with small changes to the core size used by the FPR calculations. This in turn affects the acoustic predictions. Shifting the CAMRAD/JA wake geometry away from the rotor plane by 1/4 chord produces drastic changes in the acoustic predictions indicating that the prediction of acoustic pressure is extremely sensitive to the miss distance between the vortex and the blade and that this distance must be calulated as accurately as possible for acceptable noise predictions. The inclusion or exclusion of a vortex in the FPR-RAPP calculation allows for the determination of the relative importance of that vortex as a BVI noise source. Being able to identify which vortex is responsible for the largest noise sources will lead to improved BVI noise reduction methods.

*Aerospace Engineer, Member AIAA

Introduction

Under certain flight conditions, the helicopter main rotor blade passes through or very close to the trailing tip vortices previously generated by the rotor blades. This phenomenon is referred to as blade-vortex interaction (BVI) and occurs mainly for powered descent, approach and nap-of-the-earth maneuvers. The blade-vortex interactions produce impulsive changes in blade surface pressure distributions which lead to vibration and noise problems. The BVI noise produced is highly annoying and limits the public acceptance of many helicopter applications. The reduction of BVI noise is therefore a major concern to both the rotorcraft industry and the prospective buyer.

The first step in reducing BVI noise is to understand the noise generating mechanisms. One of the first issues in the modeling of helicopter acoustics was the scalability of the BVI noise sources. It was determined that small-scale wind tunnel models could be used as tools to further the understanding of the full-scale BVI noise sources.[1,2,3] Small-scale wind tunnel models provide a major source of data to validate noise prediction efforts and have contributed to the understanding of BVI noise sources.[4-8]

BVI noise prediction techniques usually involve predicting the geometry of the vortices shed from the helicopter rotor blade tips. This information is then used to determine the blade loading, either by the use of lifting line theory or full-potential methods. The actual noise prediction methods are based on the Ffowcs Williams and Hawking equation.[9] These method require that the blade loading be supplied as input in order to predict the noise.

There is also another method of BVI noise prediction being developed. This method involves the use of the Kirchhoff equation to propagate the pressure fluctuations to the far-field. In this method, the computational fluid dynamic (CFD) solution to either the full-potential equation or the Euler equation is calculated on the Kirchhoff surface.[10] However, the rotor

tip vortex geometry must be known before-hand as input to the CFD solution.

Since all the current prediction schemes depend on either prescribed or free-wake models of the shed rotor tip vortex geometry, and there is little or no data for the core size, vortex strength and location available to validate the wake models, it is prudent to understand how the current modeling of the tip vortex affects the BVI noise predictions. One method used to evaluate the wake model is to compare the locations of the possible blade-vortex interactions as predicted by the wake model with the locations of the peak positive and negative values in the measured aerodynamic surface pressure.[11] This method determines how well the vortex model predicts the inplane geometry of the vortex, but does not indicate how well the out of plane geometry is predicted or how well the vortex core size and strength are modeled. Another method to evaluate the wake model is to use the wake model for the prediction of the rotor aerodynamic loads and the acoustics. The predicted aerodynamics and acoustics are then compared to the measured data. In this method, the discrepancies in the comparisons are due to an accumulation of errors from the vortex model, the aerodynamic prediction and the acoustic prediction. However, it can be assumed from the work documented in Refs. 12-14 that the acoustic prediction codes add little error to the end product. The results presented in these works used measured aerodynamic data as input to the acoustic codes and were in good agreement with the measured acoustic data. Therefore, the comparison of the aerodynamic predictions to the measured data provides information on how well the wake geometry model and the aerodynamic prediction scheme are performing. The comparison of the predicted acoustics, using the predicted aerodynamics, to the measured acoustics provides information about how sensitive the acoustic prediction is to errors in the wake geometry and aerodynamic models.

It is the goal of the current work to document the effect of the vortex modeling in both the wake geometry prediction program and the aerodynamic prediction program on the BVI noise predictions. Both the wake geometry and the aerodynamic prediction programs described in this paper use the Biot-Savart Law to determine the influence of the vortical velocities on the blade loading, therefore, the vortex core size is an input variable. A review of previous work documenting the effects of changing the core size will be discussed, but the main emphasis will be on the presence of a vortex and its location. Here, the vortex presence indicates whether or not a vortex trajectory is included in the aerodynamic prediction. Removing a vortex from the prediction reveals the relative importance of that vortex to the acoustic prediction.

The wake geometry model used in this paper is the Scully model in CAMRAD/JA, a comprehensive analytical model of rotor aerodynamics and dynamics by Johnson Aeronautics. FPR, a full potential rotor flow solver, incorporates the wake geometry and partial inflow angles calculated by CAMRAD/JA in the computation of the aerodynamic surface pressures. RAPP, a rotor acoustic prediction program based on the Ffowcs Williams and Hawkings equation, calculates the acoustic pressure using the FPR computed surface pressure.

The rotor aerodynamic analysis in CAMRAD/JA is based on lifting line theory with separate models for the rotor blade and the wake that are coupled by the induced velocity and the bound circulation. The rotor blade model consists of unsteady, compressible, viscous flow about an infinite aspect-ratio wing and includes corrections for yawed flow, three dimensional and unsteady effects. A lifting-surface correction is included for the first-order lifting-line theory blade-vortex interactions. The wake model consists of an incompressible vortex wake from a lifting-line with distorted wake geometry (free wake). The inboard trailed and shed vorticity is modeled using vortex sheets. The Biot-Savart Law is used to calculate the rotor wake induced velocity. The circulation in the wake is determined by the radial and azimuthal variation of the bound circulation.[15] The CAMRAD/JA computed wake geometry and inflow angles are used in FPR to solve for the aerodynamic surface pressures. Since the computational domain of FPR will include some of the wake geometry, CAMRAD/JA calculates the partial angle-of-attack, obtained by excluding the wake inside the computational domain when evaluating the non-uniform induced velocity.[15]

FPR solves the 3-D, unsteady, full potential equation for transonic flow with the density function determined by the Bernoulli equation. This rotor code, in strong conservation form, is based on the fixed-wing code of Bridgeman et al.[16] Discrete vortices are introduced into the finite-difference computations using a velocity decomposition method. The total velocity field is the sum of the gradient of the potential and the known vortex velocity.[17–19] The velocities associated with the discrete vortices are determined using the Biot-Savart Law as described by Scully in Ref. 20. The vortex is defined as a series of straight line segments with the strength varying linearly along each segment. An algebraic model is used for the solid body rotation of the vortex core. The potential equation is solved using half-point differencing formulas. First-order backward differencing is used in time and second-order differencing is used in space. The grids for the solution are a spanwise series of body fitted O-grids with 80 points in the chordwise direction, 25 points in the spanwise direction, and 25 points in the normal direction. The time step for the solution corresponds to 0.125° rotor azimuth, or about 64 time steps per chord at the rotor tip. The reason for this

relatively small time step is to capture the BVI events that happen in a very short period of time.

A simple, yet accurate rotor acoustic prediction program (RAPP) utilizes the Ffowcs Williams and Hawkings (FW-H) equation in a form well suited to incorporate blade surface pressure from computational codes such as FPR. The Lighthill stress tensor, a volume integral that models the noise produced by a non-linear flow field, is not included in the computation performed by RAPP. It is assumed in the current work that the blade-vortex interactions do not result in strong shocks and that the contribution to noise from this non-linear flow field term is negligible. RAPP can model the force terms in the FW-H equation as either compact or noncompact sources. When the chordwise compact assumption is used, the sources are distributed spanwise along the quarter chord of the acoustic planform. The source strengths are then set equal to the aerodynamic sectional coefficients calculated by FPR. When the noncompact assumption is used, the sources are distributed along the chord at each spanwise station. The source strengths are equal to the local surface pressure calculated by FPR. When experimentally measured aerodynamic surface pressure is used as input for both the compact and noncompact formulations, there is little difference in the predictions of the acoustic pressure. However, when the aerodynamic pressure from FPR is used as input, there is a noticeable difference between the acoustic pressure predicted by the two formulations. This difference in the acoustic predictions will be shown for both the 2-blade, teetering hub, AH-1/OLS model rotor and for the 4-bladed, fully articulated, UH60 model rotor.

Core Size Effects

Since both CAMRAD/JA and FPR use the Biot-Savart Law to determine the influence of the vortical velocities on the blade loading, both codes use an algebraic vortex model for the solid body rotation of the vortex core. Previous work documented the changes in the wake geometry and the partial inflow angles predicted by CAMRAD/JA when the core radius, normalized by the blade chord, was increased from $a/c = 0.046$ to $a/c = 0.20$. [21] The work was performed for the AH-1/OLS model rotor system operating at a flight condition with an advance ratio equal to 0.164, shaft tilt angle equal to 1.0 degree, hover tip Mach number of 0.665, and a thrust coefficient of 0.00535. The in-plane wake-geometry did not vary with core size and the out of plane wake geometry and vortex strength varied only slightly with core size. The partial inflow angles became a smoother function of azimuth for the increased core size. In an attempt to improve the modeling of the wake geometry by CAMRAD/JA at the inboard radial stations,

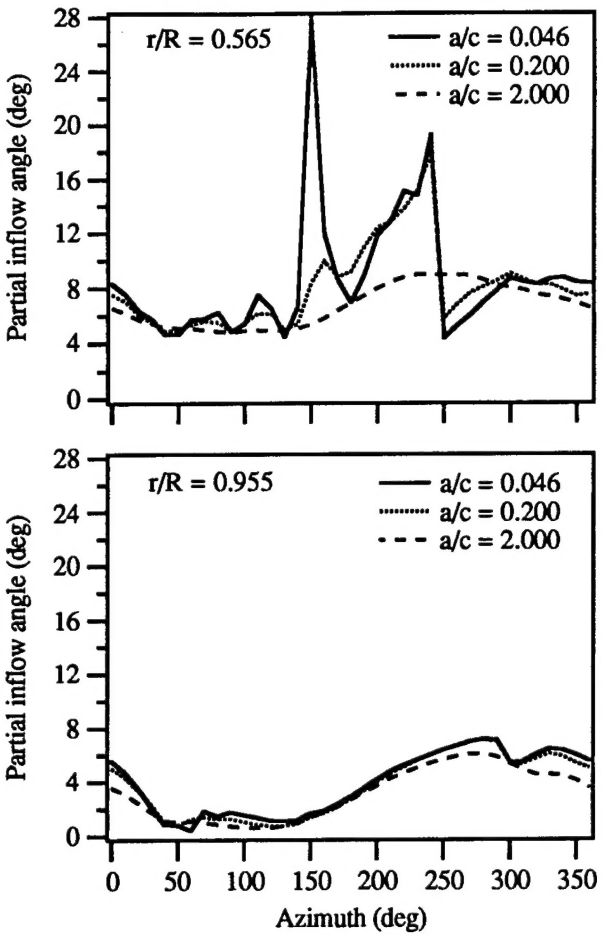

Fig. 1 CAMRAD/JA partial angles as a function of azimuth

the core size was increased drastically to $a/c = 2.0$ in the current work as recommended by Johnson Aeronautics. Even with the large increase of core size, the in-plane wake geometry did not change, and the out-of-plane wake geometry and vortex strength changed only slightly. However, there was a significant difference in the partial inflow angles predicted by CAMRAD/JA at the inboard radial stations. The difference was not as large at the outboard radial stations. The partial angles are plotted in Fig. 1 as a function of azimuth for $a/c = 0.046, 0.20$, and 2.0. Although it was not realized in the work of Ref. 21, the partial angles should not change with core size. The calculation of the partial angle should remove any vortex influence from the inflow angle. This obviously is not being accomplished and should be noted by any user of CAMRAD/JA calculated partial angles. The plots of leading edge differential pressure as a function of azimuth in Fig. 2 show the difference in the FPR calculations when using the wake geometry and partial angles from CAMRAD/JA with core sizes of $a/c = 0.20$ and $a/c = 2.0$. The core size used in FPR, $a/c = 0.20$, was the same for both cases. The

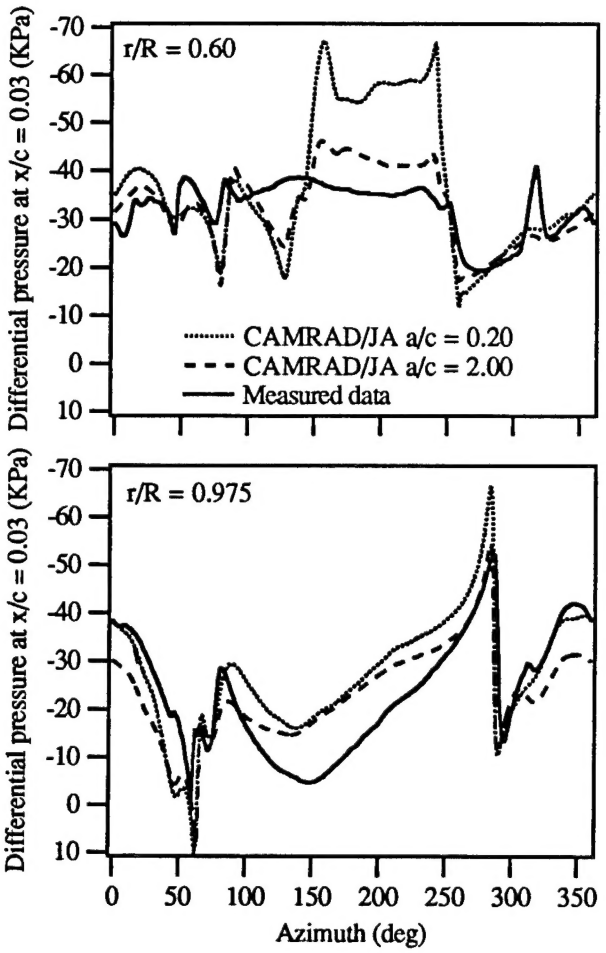

Fig. 2 Leading edge differential pressure as a function of azimuth for the AH-1/OLS model rotor. Measured data is compared to FPR calculations using partial angles from CAMRAD/JA with core sizes of a/c = 0.20 and 2.0.

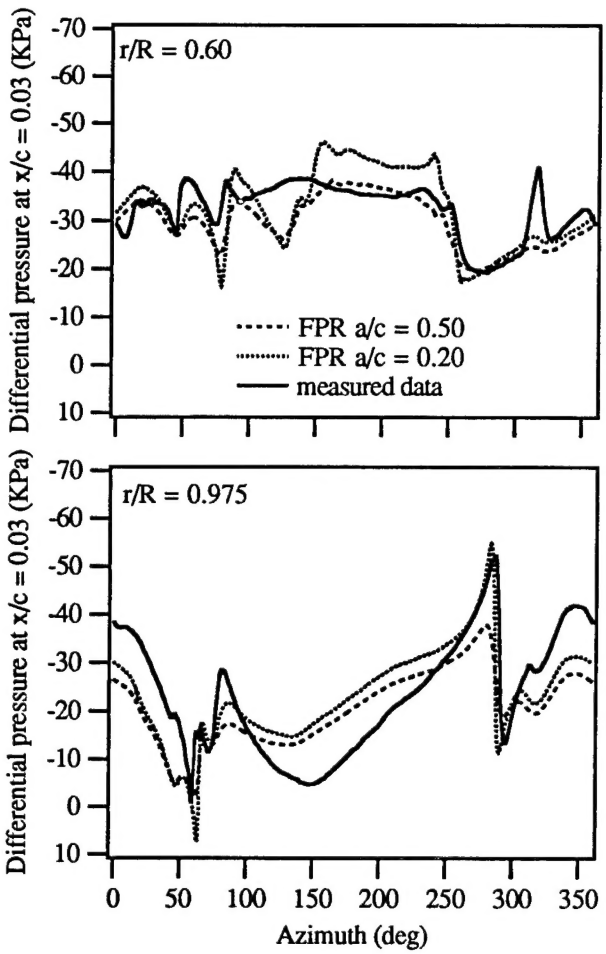

Fig. 3 Leading edge differential pressure as a function of azimuth for the AH-1/OLS model rotor. Measured data is compared to FPR calculations with core sizes of a/c = 0.20 and 0.50.

measured data for this case is also included in Fig. 2. The larger core size in CAMRAD/JA improves the prediction inboard much more than for the outboard prediction. All the following aerodynamic predictions by FPR discussed in the current paper will use input from CAMRAD/JA with a core size of $a/c = 2.0$. This does not define the core size in the FPR calculations. They are defined separately.

Changing the core size in FPR has a noticeable effect on the predicted aerodynamics and acoustics. The differential pressures near the leading edge, calculated by FPR using $a/c = 0.20$ and 0.50, are plotted as a function of azimuth in Fig. 3. The measured differential pressure is also included in Fig. 3. Increasing the core size in FPR not only reduces the amplitude, but also changes the character of the leading edge pressure. This indicates that using a larger core size in FPR to compensate for errors in miss distance defined by the CAMRAD/JA wake geometry will not result in a better prediction of the aerodynamics.

The effect of changing the core size in FPR on the acoustic predictions is shown in Fig. 4, where the acoustic pressure is plotted as a function of time for one blade passage. The measured acoustic data and the predicted acoustic data using the compact formulation of RAPP are shown for four microphone locations. All the microphones are located 1.72 rotor diameters from the rotor hub. Microphone 2 is in the plane of the rotor at 180 degrees rotor azimuth. Zero azimuth is define to be over the tail of the helicopter. Microphone 3 is 30 degrees below the rotor plane at 180 degrees rotor azimuth. Microphones 7 and 9 are also 30 degrees below the rotor plane. Microphone 7 is at 150 degrees rotor azimuth and microphone 9 is at 210 degrees rotor azimuth. The acoustic pressure is underpredicted in the rotor plane and over predicted out the plane when the core size is $a/c = 0.20$ in FPR. When the core size is $a/c = 0.50$ in FPR the acoustic pressure is underpredicted for all microphones positions. The acoustic predictions using the noncompact

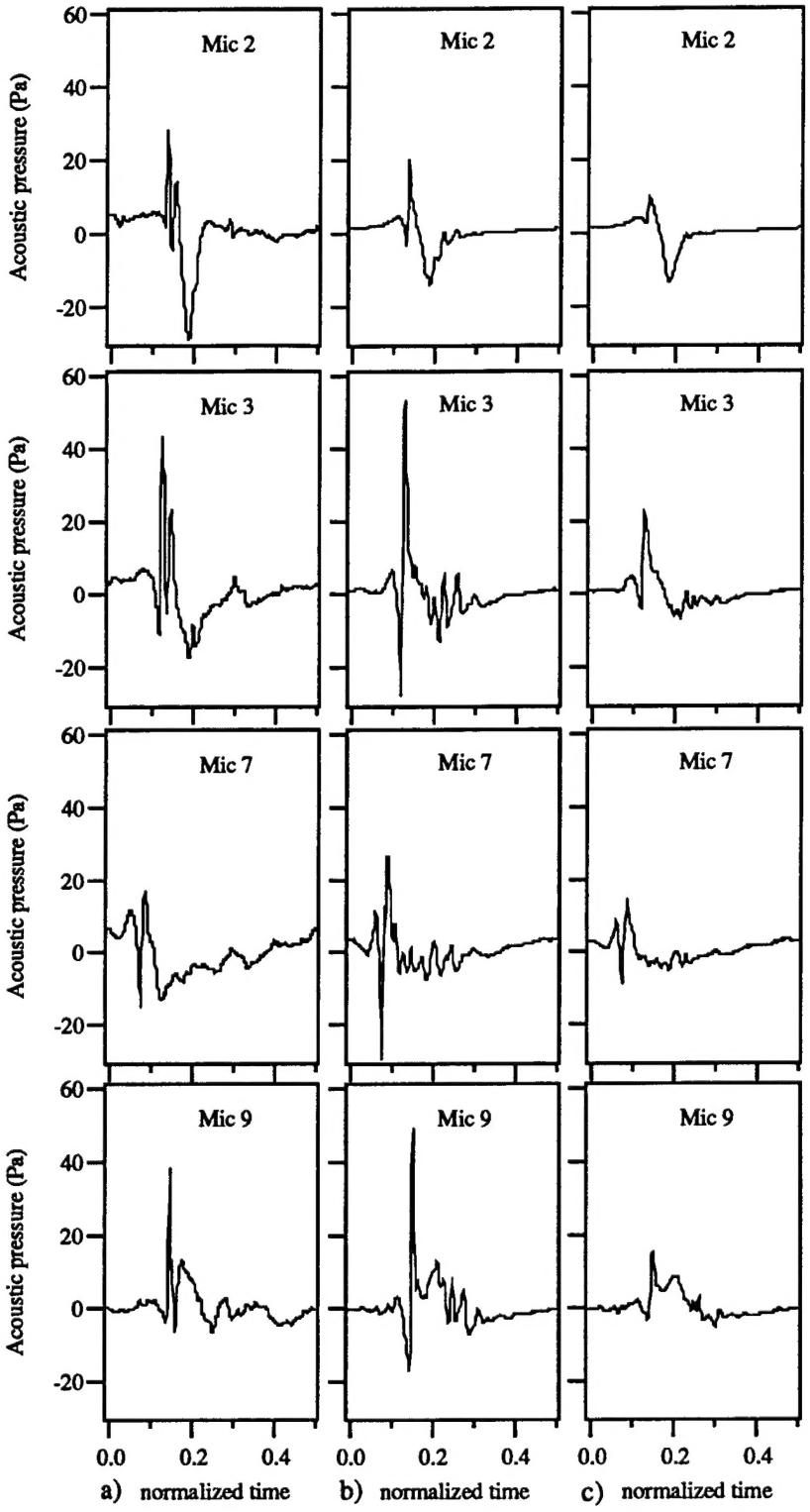

Fig. 4 Acoustic pressure is plotted as a function of normalized time (1 rev = 1 unit of time), column a) the measured acoustic pressure, column b) the acoustic pressure predicted using the compact formulation with FPR surface pressure for a/c = 0.20, and column c) the acoustic pressure predicted using the compact formulation with FPR surface pressure for a/c = 0.50.

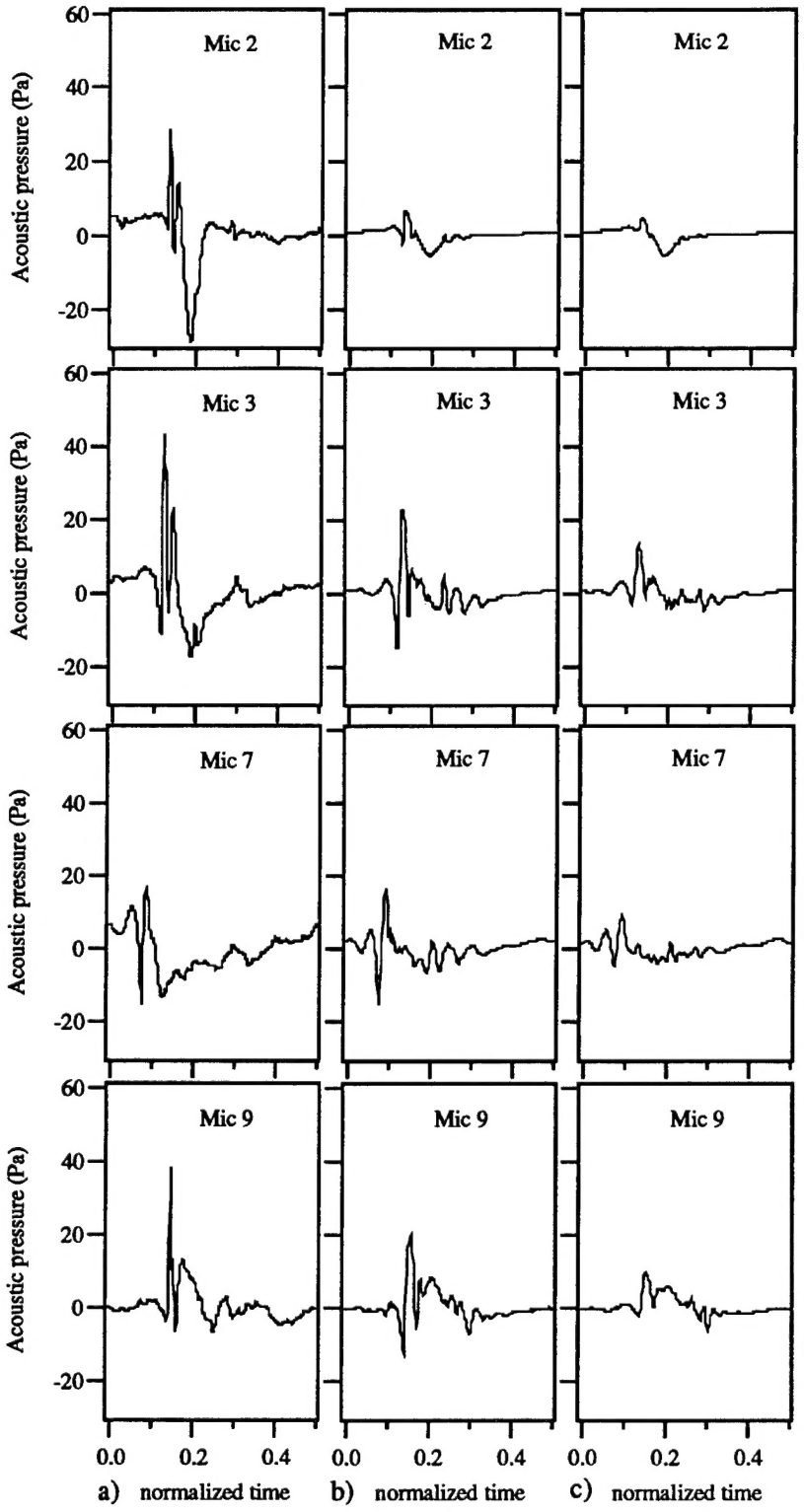

Fig. 5 Acoustic pressure is plotted as a function of normalized time (1 rev = 1 unit of time), column a) the measured acoustic pressure, column b) the acoustic pressure predicted using the non-compact formulation with FPR surface pressure for a/c = 0.20, and column c) the acoustic pressure predicted using the non-compact formulation with FPR surface pressure for a/c = 0.50.

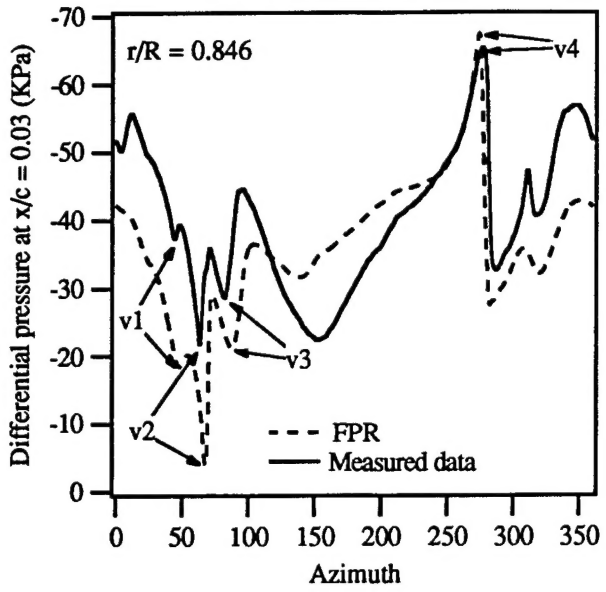

Fig. 6 Leading edge differential pressure as a function of azimuth for the AH-1/OLS model rotor. The vortex locations of interest are labeled for the measured data and the FPR prediction with a/c = 0.20

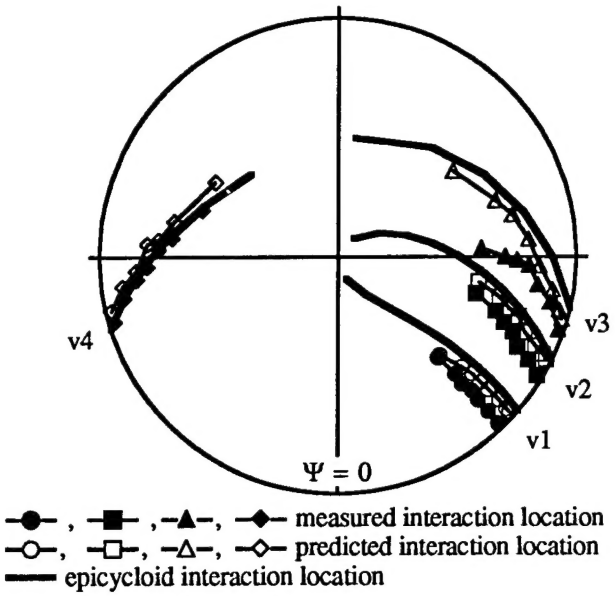

Fig. 7 Blade vortex interaction locations in the plane of the rotor for the AH-1/OLS model rotor.

formulation in RAPP are shown in Fig. 5. The measured data and acoustic predictions resulting from the core size variation in FPR are shown for the same microphone positions of Fig. 4. The acoustic predictions resulting from the noncompact formulation greatly underpredict the in-plane acoustic pressure. The out of plane predictions for $a/c = 0.20$ in FPR do not overpredict the positive pulses as is the case for the compact formulation. The positive peak is actually slightly underpredicted at microphones 3 and 9. Neither formulation is capable of predicting the second positive peak seen at microphones 2 and 3. When the core size is increased to $a/c = 0.50$ in FPR the acoustic pressure predicted by the noncompact formulation is greatly reduced.

Vortex Location

The vortex location defines the azimuth location of the interaction and the distance between the blade and the vortex at the time of the interaction. The acoustic predictions are sensitive to both the inplane location of the interaction and the miss distance. The modeling of the inplane vortex geometry by CAMRAD/JA can be evaluated by comparing the locations of the positive and negative peaks in the leading edge differential pressure from the FPR predictions to the locations of the positive and negative peaks in the measured leading edge differential pressure. The negative peaks indicate the location of the BVI on the advancing side and the positive peaks indicate the location of the BVI on the retreating side. The leading edge pressures are plotted in Fig. 6 for a radial station of r/R = 0.846 with the vortex locations of interest labeled as v1, v2, v3 and v4. Both the predicted and measured pressures are shown in Fig. 6 for the same 2-bladed rotor case described above. The locus of interaction locations for each vortex is plotted in Fig. 7 along with the calculation of all the possible interactions of the blade with the epicycloid representing the vortex trajectory. The epicycloid vortex trajectory does not take into account any convection of the vortex by induced flow fields. The CAMRAD/JA-FPR predicted interaction locations on the advancing side of the rotor fall between the epicycloid and the measured interaction locations. This indicates that CAMRAD/JA is modeling some convection from flow of one vortex induced on another, but that this modeling is not adequate. The incorrect prediction of the inplane location of the BVI could account for why the acoustic prediction is missing the second peak of microphone 3 in both Figs. 4 and 5.

The prediction of the wake geometry becomes more complicated for a four bladed rotor system. The CAMRAD/JA-FPR prediction of the leading edge differential pressure at r/R = 0.92 is compared to the experimentally measured leading edge differential pressure at r/R = 0.92 in Fig. 8 for the UH-60 model rotor tested in the DNW.[6] The operating conditions for the BVI test case shown in Fig. 8 are an advance ratio of 0.15, hover tip Mach number of 0.64, and thrust coefficient of 0.0045. The positive and negative peaks have been identified as in Fig. 6. There is obviously a phase difference between the identified

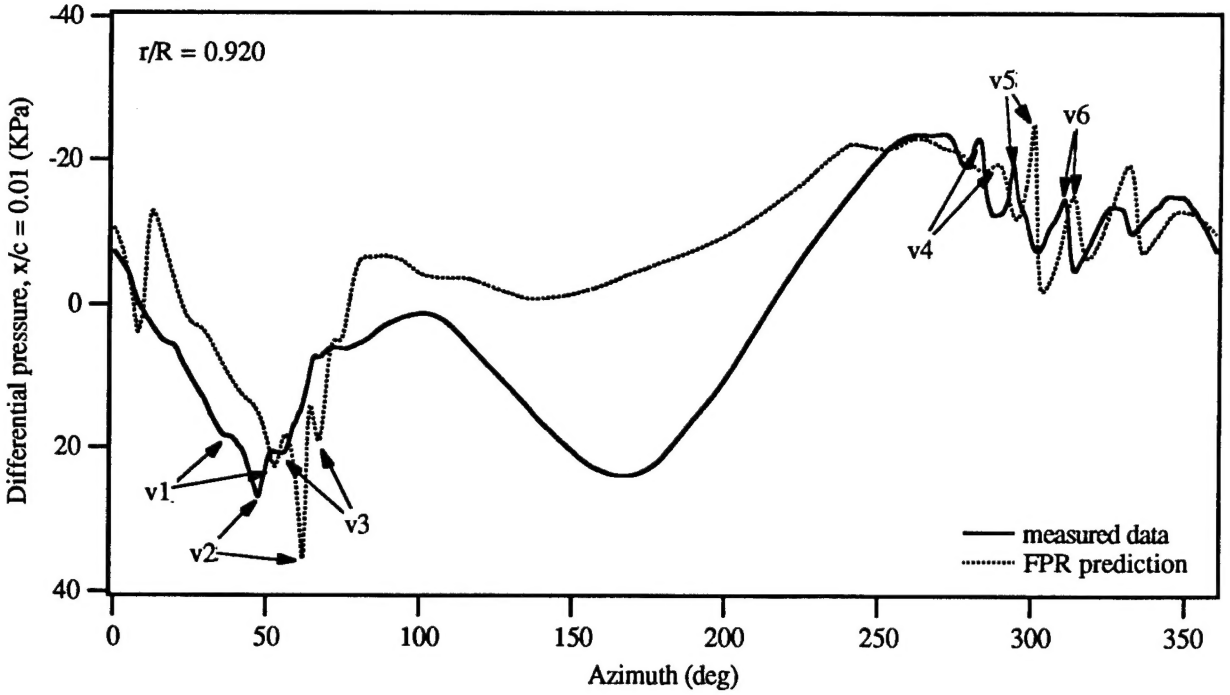

Fig. 8 Leading edge differential pressure as a function of azimuth for the UH60 model rotor. The vortex locations of interest are labeled for both the measured data and the FPR prediction with a/c = 0.20

peaks in the measured data and the identified peaks in the CAMRAD/JA-FPR prediction.

The locus of interaction locations for each vortex is shown in Fig. 9 along with the calculated positions of all the possible interactions of the blade with the epicycloid representing the vortex trajectory. On the advancing side of the rotor, the predicted BVI locations correspond to the BVI locations of the epicycloid trajectory. Whereas the measured BVI locations occur between or cross over the BVI locations of the epicycloid trajectory. This indicates that there is a large effect of induced velocity on the location of the vortex interaction that is not being calculated correctly by CAMRAD/JA. The effect of the induced velocity is much larger for four the 4-bladed rotor than for the 2 bladed rotor. This is because there are more vortices for the 4-bladed rotor in a similar region as for the 2-bladed rotor. Therefore, the vortices are in closer proximity and exert a greater influence on one another.

The phase shift between the measured BVI locations and the predicted BVI locations (see Fig. 8) indicates that the out-of-plane prediction of the vortex location by CAMRAD/JA is not correct. Fig. 10 displays the predicted wake geometry within the computational domain when the rotor is at 55 degrees azimuth. The segments of the vortex trajectories are projected both in the plane of the rotor and in a plane perpendicular to the rotor. The rotor blade and computational domain are also shown in Fig. 10. The

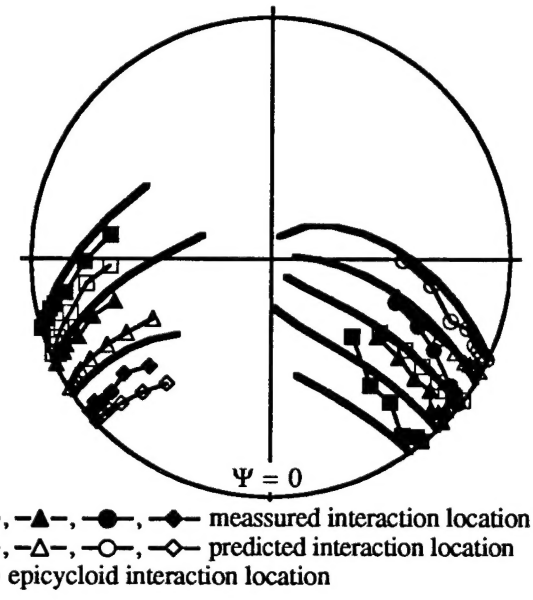

Fig. 9 Blade vortex interaction locations in the plane of the rotor for the UH60 model rotor.

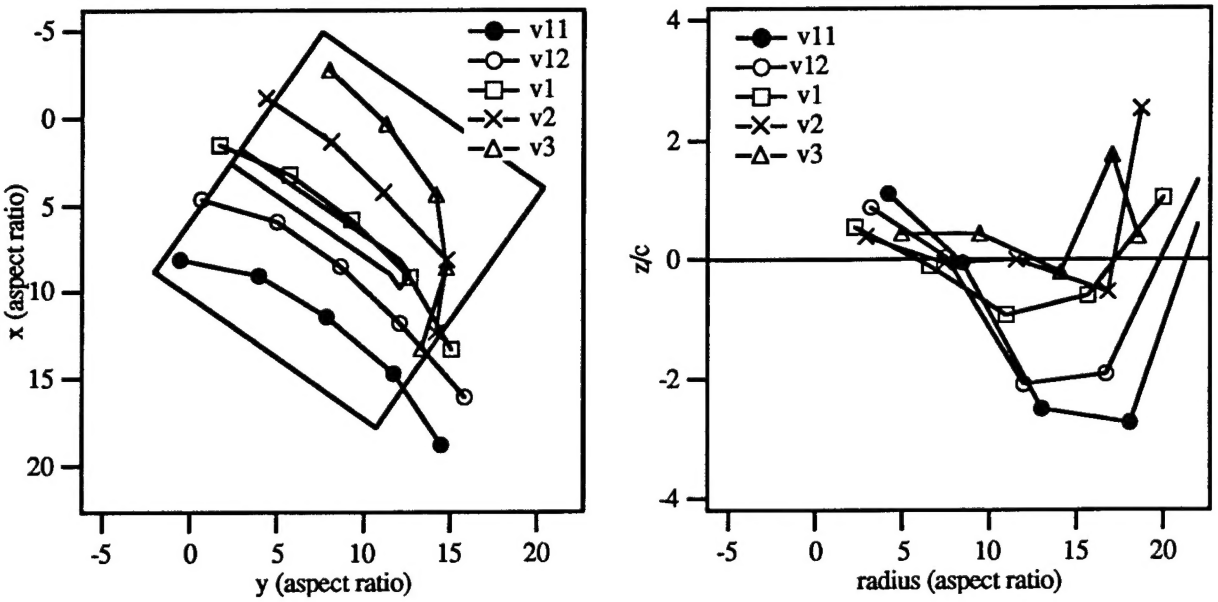

Fig. 10 CAMRAD/JA predicted wake geometry at 55 degrees azimuth for the UH60 model rotor.

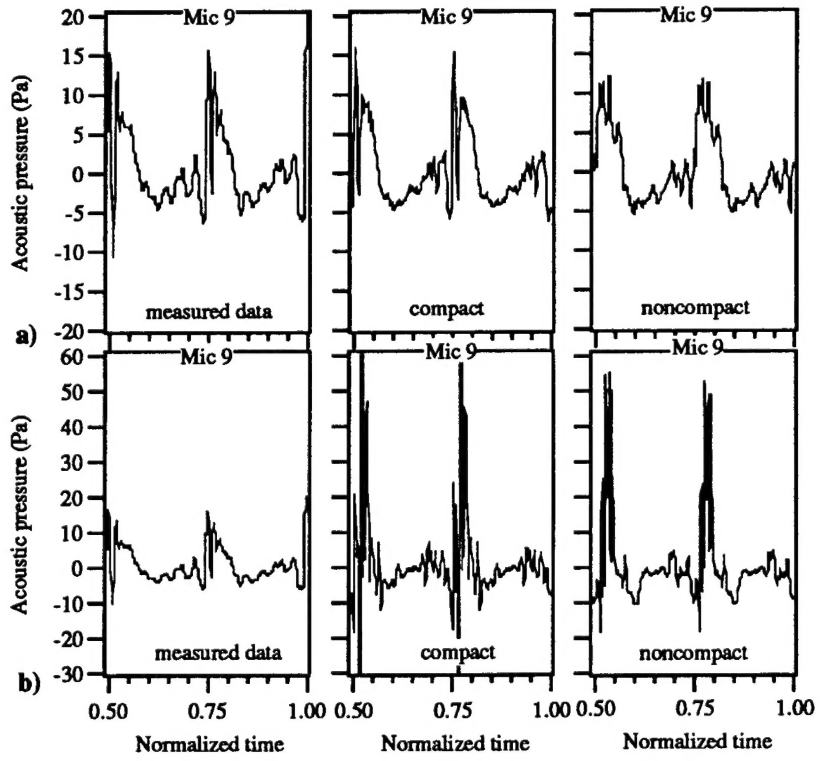

Fig. 11 Acoustic pressure is plotted as a function of normalized time (1 rev = 1 unit of time), row a) measured acoustic data compared to acoustic prediction using compact and non-compact formulations with measured surface pressure, row b) measured acoustic data compared to acoustic prediction using compact and non-compact formulations with FPR predicted surface pressure.

comparison of measured and calculated leading edge pressure (see Fig. 8) suggests that vortices v2 and v3 in Fig. 10 are too close to the rotor whereas vortices v11 and v12 are too far from the rotor.

The acoustic predictions for this UH-60 case are compared to the measured data in Fig. 11 for microphone 9 which is 3.0 rotor radii from the hub and 25 degrees below the rotor plane at 150 degrees rotor azimuth. Both the compact and noncompact formulations have been included for the predictions using measured surface pressure and for the predictions using FPR calculated surface pressure. Both the compact and noncompact formulations, when using measured surface pressure, compare well with measured data. However, both acoustic formulations using the FPR calculated surface pressure overpredict the BVI noise. The poor comparison to the measured data is a direct result of the incorrect modeling of the wake geometry.

To see how sensitive the acoustic predictions are to the miss distance at the time of interaction, the out-of-plane location predicted by CAMRAD/JA was shifted down 0.25 chords and 0.5 chords then used by FPR to predict the surface pressures. The effect of miss distance on the prediction of the surface pressures is shown in Fig. 12 for the 2-bladed AH-1/OLS rotor case discussed above at radial stations of r/R = 0.846 and 0.91 and a chordwise station of x/c = 0.03. The FPR results shown in Fig. 12 include the predictions using the unshifted CAMRAD/JA wake geometry and the predictions using the CAMRAD/JA wake geometry shifted 0.25 chords and 0.5 chords. The vortex labeled v1 in Fig. 12 is only slightly affected by the shift in the vortex geometry at either radial station. Vortices v2, v3 and v4 are all significantly affected by the geometry shift. The amplitude of vortex v2 is reduced while the amplitude of v3 is increased because v2 was below the plane of the rotor and was moved farther from the blade with the downward shift and v3 was above the plane of the rotor and was moved closer to the blade with the downward shift. The effect of changing the miss distance on the predicted acoustic pressure is shown in Fig. 13, where the compact acoustic formulation was used, and in Fig. 14, where the non-compact acoustic formulation was used. For both formulations, the major acoustic pulse is reduced while the following pulses are increased. The increase in the secondary pulses is most evident for the 0.25 chord shift. The predictions in Figs. 13 and 14 indicate that the acoustic predictions are quite sensitive to small shifts in the wake geometry.

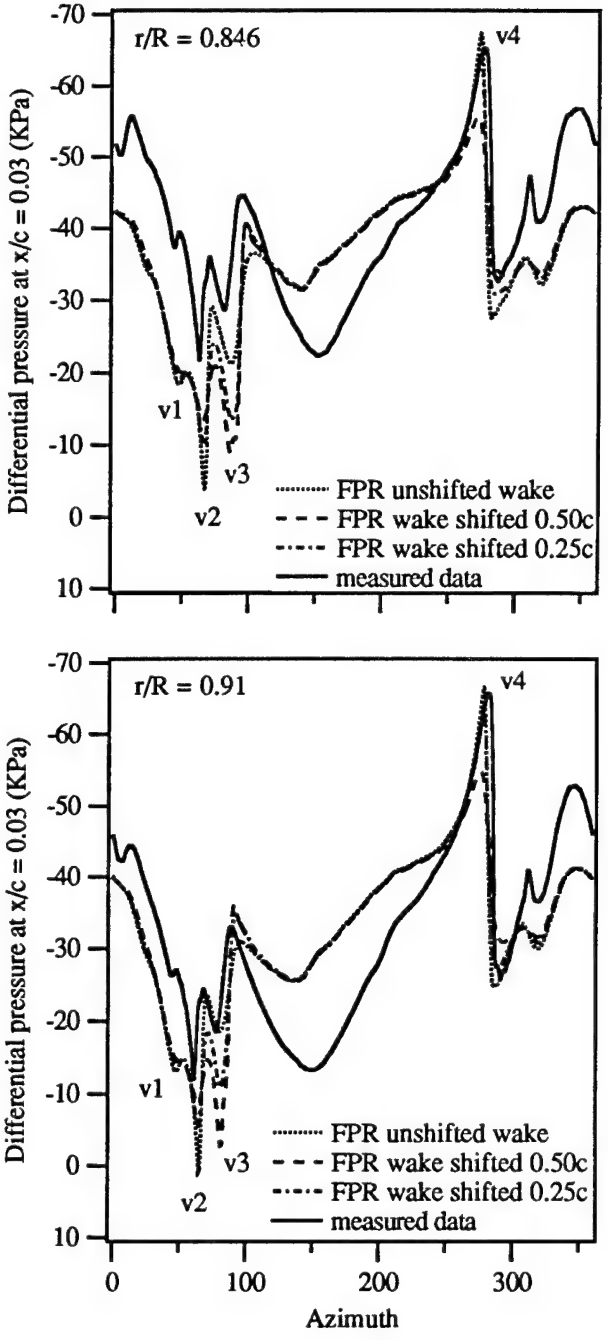

Fig. 12 Leading edge differential pressure as a function of azimuth for the AH-1/OLS model rotor. The measured data is compared to FPR predictions for an unshifted wake and for the wake shifted away from the rotor 0.25c and 0.50c.

Vortex Presence

Being able to determine which blade-vortex interaction produces the most noise is valuable knowledge that could lead to major noise reduction. One

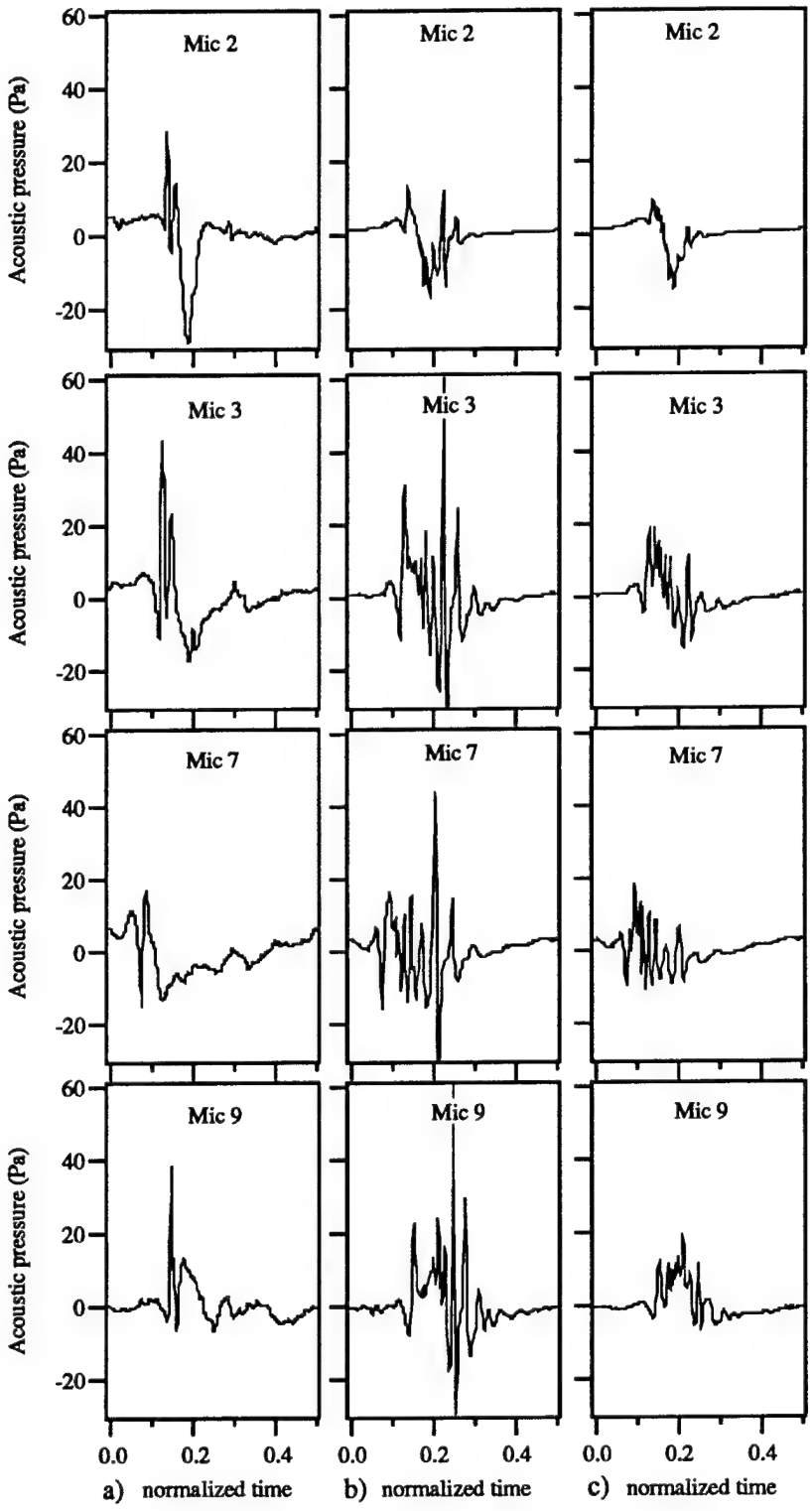

Fig. 13 Acoustic pressure is plotted as a function of normalized time (1 rev = 1 unit of time), column a) the measured acoustic pressure, column b) the acoustic pressure predicted using the compact formulation with FPR surface pressure with the wake shifted 0.25c, and column c) the acoustic pressure predicted using the compact formulation with FPR surface pressure with the wake shifted 0.50c.

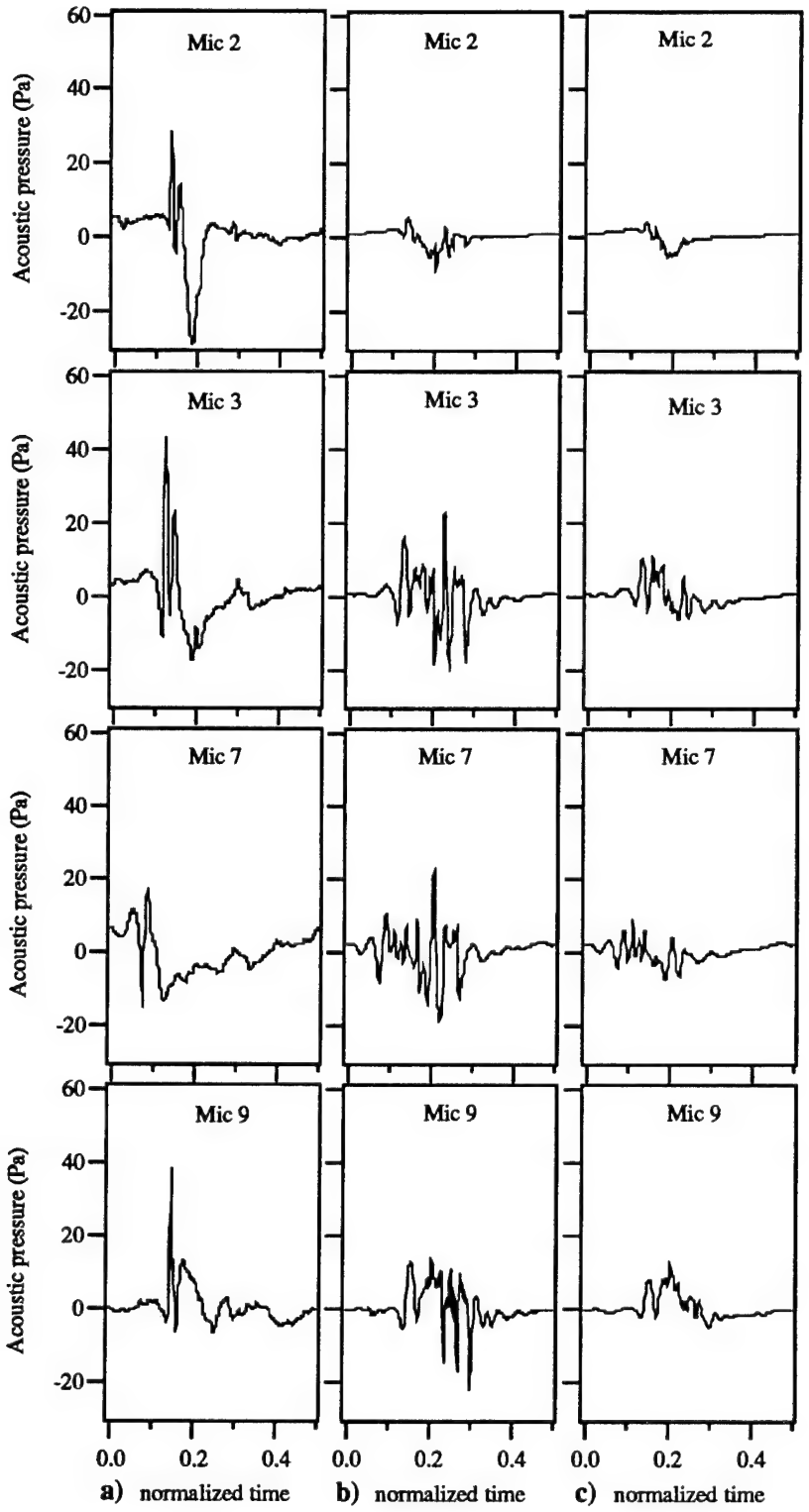

Fig. 14 Acoustic pressure is plotted as a function of normalized time (1 rev = 1 unit of time), column a) the measured acoustic pressure, column b) the acoustic pressure predicted using the non-compact formulation with FPR surface pressure with the wake shifted 0.25c, and column c) the acoustic pressure predicted using the non-compact formulation with FPR surface pressure with the wake shifted 0.50c.

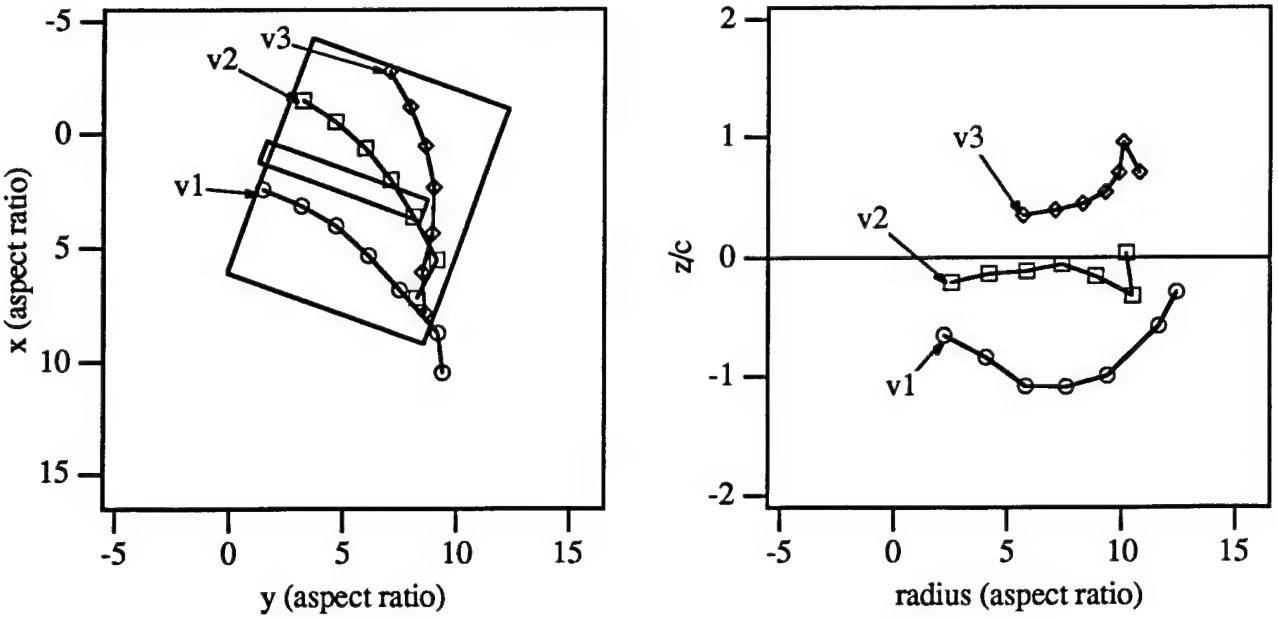

Fig. 15 CAMRAD/JA predicted wake geometry at 70 degrees azimuth for the AH-1/OLS model rotor.

technique that is available only to the prediction methods is to remove vortices from the computation. The extent that the acoustic predictions are affected by the vortex removal indicates the relative importance of that vortex to the noise signature. This procedure was preformed for the 2-bladed AH-1/OLS model rotor discussed previously. There are three vortex trajectories included in the computation performed by FPR. The segments of these trajectories that are within the computational domain when the rotor is at 70 degrees rotor azimuth are shown in Fig. 15, which is a snapshot of the vortex segments at a single instant. The purpose of Fig. 15 is to clarify which vortex is being removed from the computation. Fig. 16 shows the effect of removing the vortices from the computation on the leading edge differential pressure. The vortices have been labeled to match the labeling of Fig. 6. The interactions can be removed from the calculated pressure by removing a vortex trajectory from the computation. In two cases, removing one vortex trajectory actually removes an interaction from both the advancing side and the retreating side, indicating that the vortex trajectory has segments in the computational domain on both sides of the rotor disk.

The effect of removing the vortex trajectories from the computation on the acoustic predictions is shown in Figs. 17 and 18. In Fig. 17, the compact formulation is used to predict the acoustics and in Fig. 18, the non-compact formulation is used. These plots can be compared to the first two columns of Figs. 4 and 5 which show the measured acoustic data and the acoustic predictions using the same core size and vortex positions used for the vortex removal calculations. Removing the second vortex trajectory removes the largest interaction from the FPR predictions shown in Fig. 16 and also removes the largest interaction from the acoustic predictions in Figs. 17 and 18. This excersize illustrates the ability to identify the BVI noise sources.

Concluding Remarks

Most of the current BVI noise prediction schemes rely on prescribed-wake or free-wake models to define the vortex location and strength of the tip vortices. The current work shows that there can be no compensating for the discrepancies in the wake model when attempting to accurately predict the BVI noise. More specifically, errors in modeling the vortex location can not be compensated for by adjusting the core size in the viscous core model. This paper discusses the effects of modeling the core size in both CAMRAD/JA and FPR on the acoustic predictions. The most important result of varying the core size in CAMRAD/JA is that CAMRAD/JA does not accurately remove the vortex influence from the inflow angles when calculating the partial angles. Otherwise, changing the core size in CAMRAD/JA has little affect on the wake geometry or the predicted acoustics. The aerodynamic surface pressure predicted by FPR is quite sensitive to the core size used for the predictions. This in turn greatly affects the acoustic predictions that use the FPR predicted surface pressure. For both the 2-bladed and 4-bladed rotor systems discussed in this paper, CAMRAD/JA did not adequately model the convection of the vortex trajectories caused by induced flow that is produced by nearby vortex trajectories. The error in

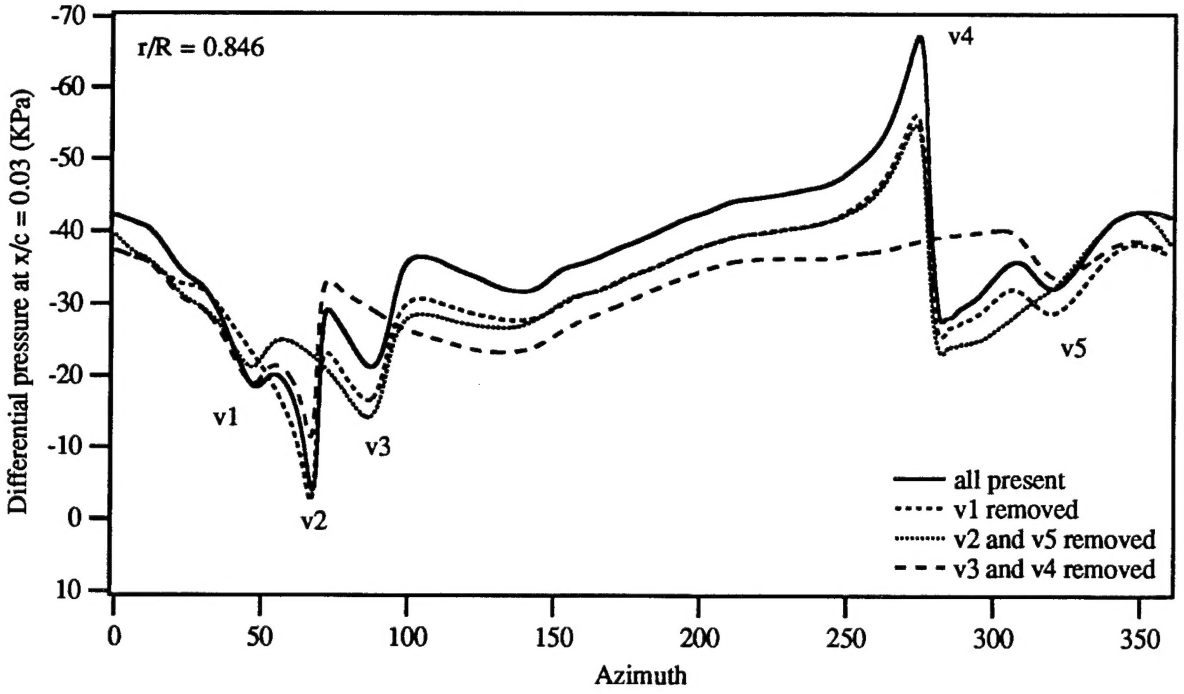

Fig. 16 Leading edge differential presssure as a function of time for the AH-1/OLS model rotor. The FPR predictions are shown with all the vortices present in the computation and with v1 removed, v2 and v5 removed, and v3 and v4 removed.

modeling the vortex convection produces errors in the vortex location with respect to the blade. The results of this paper show that both the aerodynamic and acoustic predictions are quite sensitive to small errors in the vortex locations.

The BVI noise prediction schemes can be quite useful when they work relatively well. The current work shows that the inclusion or exclusion of a vortex in the FPR-RAPP calculation allows for the determination of the relative importance of that vortex as a BVI noise source. Being able to identify which vortex is responsible for the largest noise source will lead to improved BVI noise reduction methods.

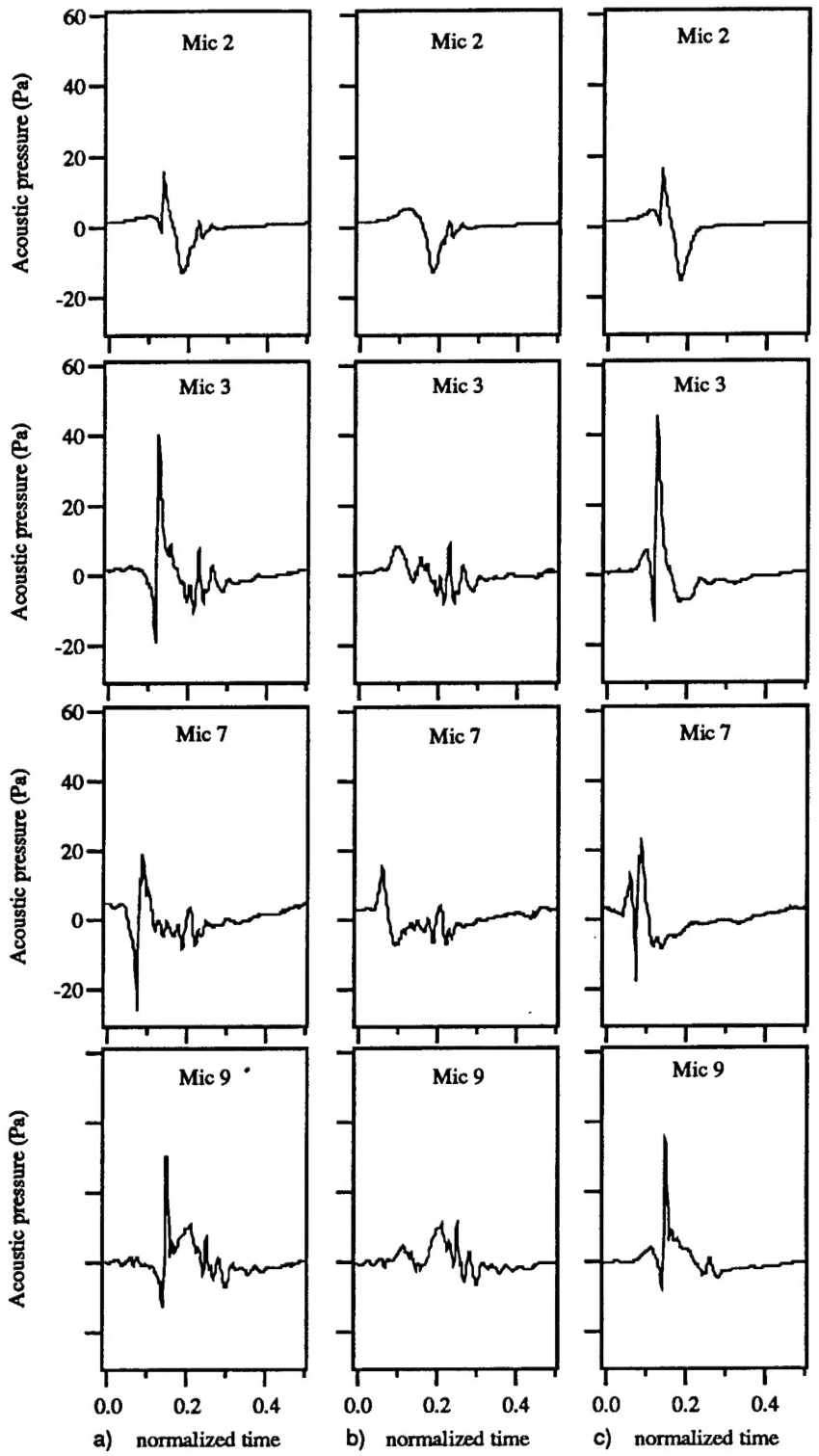

Fig. 17 Acoustic pressure predicted using the compact formulation is plotted as a function of normalized time (1 rev = 1 unit of time), column a) v1 removed from the FPR computation,column b) v2 and v5 removed from the FPR computation, and column c) v3 and v4 removed from the FPR computation.

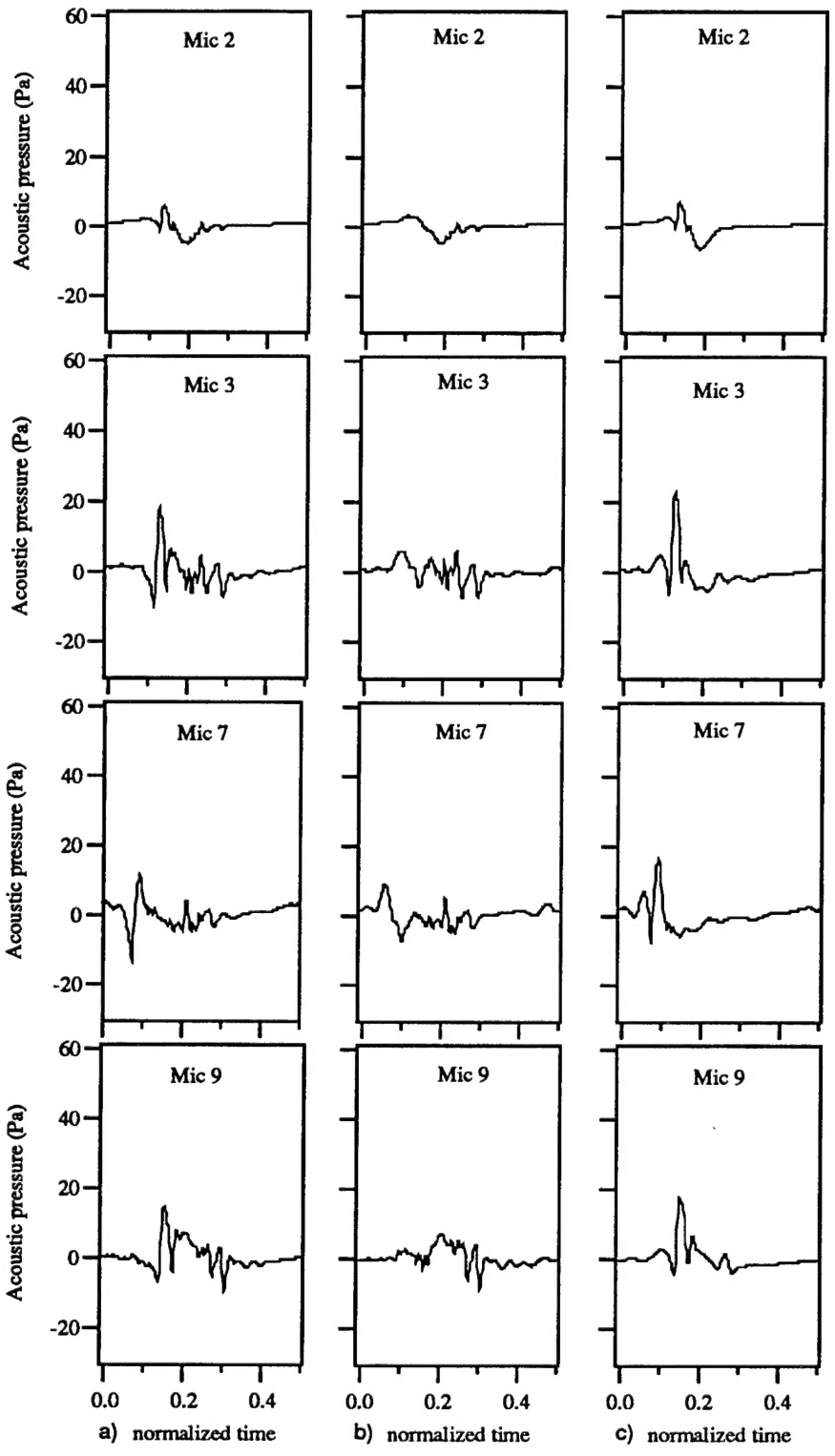

Fig. 18 Acoustic pressure predicted using the noncompact formulation is plotted as a function of normalized time (1 rev = 1 unit of time), column a) v1 removed from the FPR computation, column b) v2 and v5 removed from the FPR computation, and column c) v3 and v4 removed from FPR computation.

References

[1]Schmitz, F.H., Boxwell, D.A., Lewy, S., and Dahan, C., "A Note on the General Scaling of Helicopter Blade-Vortex Interaction Noise," *American Helicopter Society 38th Annual National Forum Proceedings,* Anaheim, CA, May 1982.

[2]Splettstoesser, W.R., Schultz, K.J., Schmitz, F.H., and Boxwell, D.A., "Model Rotor High Speed Impulsive Noise - Parametric Variations and Full-Scale Comparisons," *American Helicopter Society 39th Annual National Forum Proceedings,* St. Louis, MO, May 1983.

[3]Boxwell, D.A., Schmitz, F.H., Splettstoesser, W.R., and Schultz, K.J., "Helicopter Model Rotor-Blade Vortex Interaction Impulsive Noise: Scalability and Parametric Variations," *Journal of the American Helicopter Society,* Vol. 32, No. 1, Jan. 1987.

[4]Dadone, L., Dawson, S., Boxwell, D., and Ekquist, D., "Model 360 Rotor Test at DNW - Review of Performance and Blade Airload Data, *American Helicopter Society 43rd Annual Forum Proceedings,* St. Louis, MO, May 1987.

[5]Zinner, R.A., Boxwell, D.A., and Spencer, R.H., "Review and Analysis of the DNW/Model 360 Rotor Acoustic Data Base," *Proceedings of the 15th European Rotorcraft Forum,* Amsterdam, the Netherlands, Sept. 1989.

[6]Lorber, P.F., "Aerodynamic Results of a Pressure-Instrumented Model Rotor Test at the DNW," *American Helicopter Society 46th Annual Forum Proceedings,* Washington, D.C., May 1990.

[7]Liu, S.R, and Marcolini, M.A., "The Acoustic Results of a United Technologies Scale Model Rotor Tested at the DNW," AIAA 13th Aeroacoustics Conference, Tallahassee, FL, Oct. 1990.

[8]Yu, Y.H, Gmelin, B., Heller, H., Phillipe, J.J., Mercker, E., and Preisser, J.S., "HHC Aeroacoustic Rotor Test at the DNW - The Joint German/French/US HART Project," *Proceedings of the 20th European Rotorcraft Forum,* Amsterdam, The Netherlands, Oct. 1994.

[9]Ffowcs Williams, J.E., and Hawkings, D.L, "Sound Generation by Turbulence and Surfaces in Arbitrary Motion," *Philosophical Transaction of the Royal Society of London,* Series A, Vol. 264, No. 1151, May 8, 1969, pp. 321-342.

[10]Xue, Y. and Lyrintzis, A. S., "Rotating Kirchhoff Method for Three Dimensional Transonic Blade-Vortex Interaction Hover Noise," *AIAA Journal,* Vol. 32, No. 7, July 1994.

[11]Marcolini, M.A., Martin, R.M., Lorber, P.F, and Egolf, T.A., "Prediction of BVI Noise and Correlation with Wake Interaction Locations," *American Helicopter Society 48th Annual Forum Proceedings,* Washington, D.C., June 1992.

[12]Schultz, K.J., "Prediction of Helicopter Rotor Impulsive Noise Using Measured Blade Pressures," *American Helicopter Society 43rd Annual Forum Proceedings,* St. Louis, MO, May 1987.

[13]Gallman, J.M., "The Validation and Application of a Rotor Acoustic Prediction Program," *Proceedings of the 1990 Army Science Conference,* Durham, NC, June 1990.

[14]Visintainer, J.A., Burley, C.L., Marcolini, M.A., and Liu, S.R., "Acoustic Predictions Using Measured Pressure from a Model Rotor in the DNW," *American Helicopter Society 47th Annual Forum Proceedings,* Phoenix, AS, May 1991.

[15]Johnson, W., "CAMRAD/JA A Comprehensive Analytical Model of Rotorcraft Aerodynamics and Dynamics," Johnson Aeronautics, Palo Alto, California, 1988.

[16]Bridgeman, J. O., Steger, J. L. , and Caradonna, F. X., "A Conservative Finite-Difference Algorithm for the Unsteady Transonic Potential Equation in Generalized Coordinates," AIAA Paper 82-1388, Aug. 1982.

[17]Strawn, R., Tung, C., "The Prediction of Transonic Loading on Advancing Helicopter Rotors," NASA TM 88238, US AVSCOM TM 886-A-1, April 1986.

[18]Strawn, R.C., and Caradonna, F.X., "Conservative Full-Potential Model for Unsteady Transonic Rotor Flows," *AIAA Journal,* Vol. 25, No. 2, Feb. 1987, p.193.

[19]Caradonna, F.X., and Strawn, R.C., "An Experimental and Computational Study of Rotor-Vortex Interaction," *Vertica,* Vol. 12, No. 4, 1988, pp. 314-327.

[20]Scully, M.P., "Computation of Helicopter Rotor Wake Geometry and Its Influence on Rotor Harmonic Airloads," ASRL TR-178-1, Massachusetts Institute of Technology, March 1975.

[21]Gallman, J.M., Tung, C., Yu, Y.H., and Low, S.L., "Prediction of Blade-Vortex Interaction Noise with Applications to Higher Harmonic Control," AIAA-93-4331, 15th Aeroacoustics Conference, Long Beach, CA, Oct. 1993.